VOL. 12, NO. 20, OCTOBER 2017 ISSN 1819-6608
ARPN Journal of Engineering and Applied Sciences

www.arpnjournals.com

THE S-S CURVE APPROXIMATION FOR GFRP TENSILE SPECIMEN BY USING INVERSE METHOD AND OPTIMIZATION

D. S. Shin and E. S. Jeon
Department of Mechanical Engineering, Kongju National University, Korea
E-Mail: osjun@kongju.ac.kr

ABSTRACT

Improving the accuracy of FEA on composite material parts to reduce weight is an important issue in industry and academia. The mechanical properties of composite materials have generally been studied from a microscopic perspective. The properties of relatively large or complicated models need to be identified on a macroscopic scale. However, only a few studies were performed on an inverse method that presents a plastic region as a simple model. This study proposed a method to reduce errors with respect to experimental data by presenting the mechanical properties using the inverse method and performing parameter optimization for the inverse method to realize the axial displacement of GFRP tensile specimens by FEA.

Keywords: GFRP, tensile test, inverse method, non-linear analysis, DOE.

INTRODUCTION

The true strain-true stress curve (true s-s curve) after the yield point of a certain material is a critical factor that must be obtained to improve the reliability of the FEA step for products that undergo plastic deformation or high energy absorption [1]. The mechanical properties that are generally used for FEA can be identified through a tensile test like ASTM D638-02a [2]. However, engineering strain-engineering stress curve (eng. s-s curve) data only can be obtained with a general tensile test, and plastic deformation of the center cross-section is not taken into account during the tensile test. Therefore, the result of FEA when the eng. s-s curve was applied had reduced accuracy. True s-s curves considering the cross-section change in a tensile test specimen can be calculated by the direct method and inverse method. The direct method allows obtaining the true s-s curve of a specimen's cross-section area directly, as in the precision measuring instrument applied in the study by Iadicola [3] and the vision measurement systems employed in the studies of Geiger [4], Zhu [5], and Kim [6]. Under the direct method, the instrument for measuring the cross-section area becomes more expensive when its measurement error and instrument errors are improved. Further, the direct method cannot be applied to general tensile tests. When the inverse method is applied, the eng. s-s curve obtained with the tensile test is processed as the true s-s curve through mathematical modeling, as shown by Joun [7], Kamaya [8], and Zhao [9]. However, to improve accuracy, the parameters of the inverse method should be regenerated based on the materials. It is particularly difficult to carry out mathematical modeling of fiber direction and density in GFRP produced by injection molding. Therefore, studies were performed for identifying the properties of samples with artificial fiber orientation [10] or for obtaining the local properties with the experimental realization of simple and similar models [11]. Nevertheless, the above methods were applied to studies at the microscopic scale. Moreover, they could not address the problem that the mechanical properties changed significantly depending on factors such as fiber orientation, injection molding, and the injection-molded shape. The properties of composite materials should also be identified and predicted macroscopically as needed. Unal [12] proposed a method to analyze the uniaxial material properties of complicated shapes, large models, or composite materials whose ratio of internal materials can be changed using fuzzy theory and tests in the macroscopic perspective. However, the inverse method was not proposed, and the parameter optimization process was not taken into account. Therefore, one cannot expect accuracy in the material properties. If the ratio of internal materials is not considered, the inverse method is suggested from the macroscopic perspective, and the parameter optimization process is also presented to reduce errors. Tithe material properties of the composite materials can be modeled like general metals and applied to FEA.

This study predicted the properties of a GFRP wt20%GF tensile specimen (a material that is light and widely used for car parts) with the inverse method and proposed a method to reduce the error by applying parameter optimization when the inverse method for metal was inappropriate for the GFRP. To achieve the goal, the eng. s-s curve for the GFRP was obtained through a tensile test, and an error range was proposed when the eng. s-s curve was applied to FEA with the inverse methods. Then, optimization was applied to reduce the error range of the proposed inverse method. The inverse method and parameters that are the closest approximations to the test results were proposed.

2. TRUE S-S CURVE MODEL

2.1 ASTM D638-02a test

The test equipment consisted of a tensile testing machine, a measurement instrument to obtain data, and a PC to collect and analyze the data (Figure-1). The specimen was fixed at both ends with a grab and displacement at a speed of 5 mm/min was applied. The specimen tested with the tensile testing machine was a GFRP wt20%GF tensile specimen of dog-bone type according to ASTM D638-02a; the gauge length was

measured with a strain gauge to measure the strain precisely.

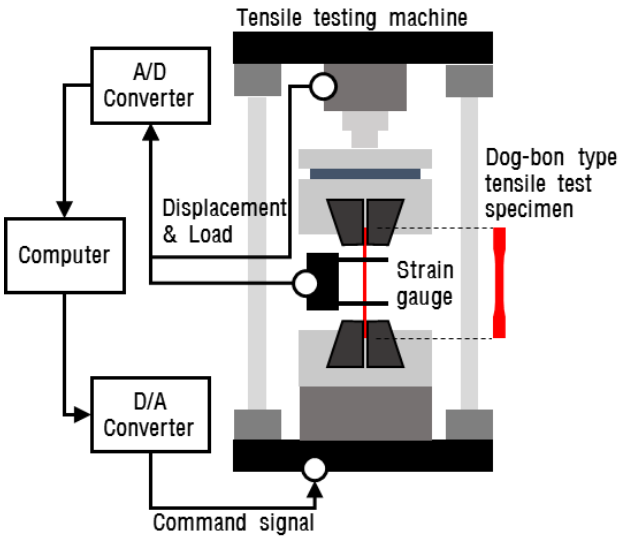

Figure-1. Diagram based on the ASTM D638-02a test.

Table-1. The material properties of GFRP.

Symbols	Description	Values	Units
E	Young's modulus	3388	MPa
ν	Poisson's ratio	0.43	-
A	Section area	41.6	mm^2
L_o	Gauge distance	50	mm

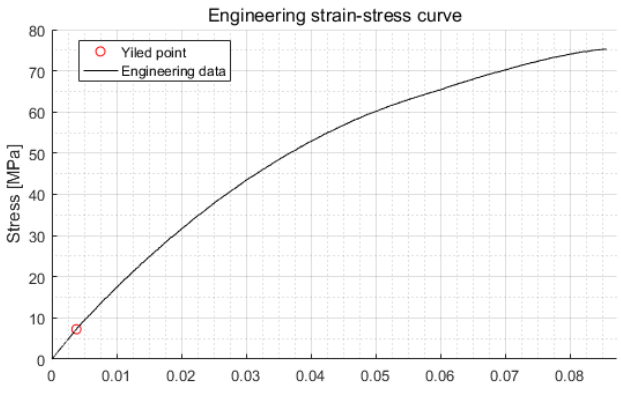

Figure-2. The eng. s-s curve data.

When the initial cross-section area of the specimen center was A_c, the external force (changing with time) was F, the gauge length was L_c, the gauge length change with external force was ΔL_c, and the gauge length at a given time was L, the engineering strain(ε_c) and engineering stress(σ_c) could be calculated as follows.

$$\varepsilon_o = \Delta L/L_o = (\mathrm{L} - \mathrm{L_o})/L_o \quad (1)$$

$$\sigma_o = F/A_o \quad (2)$$

When the cross-section area that changed with time was assumed as (blank), the true strain (ε_T)-true stress (σ_T)relationship could be described by the following equation.

$$\epsilon_T = \int_{L_o}^{L} \Delta L/L = ln(L/L_o) \quad (3)$$

$$\sigma_T = F/A = \sigma_o(1+\varepsilon_o) = \sigma_o(L/L_o) \quad (4)$$

2.2 Inverse method

The yield point could be calculated from Young's modulus and the engineering s-s curve. The area before the yield point is called the elastic area, while the area after the yield point is the plastic region; the data in the plastic region were significantly dealt with by the inverse method.

$$\sigma_T = K\varepsilon_o^n \quad (5)$$

$$\sigma_T = c + K\varepsilon_o^n \quad (6)$$

$$\sigma_T = K(c+\varepsilon_o)^n \quad (7)$$

Under the inverse method, the eng. s-s curve obtained through the test was theoretically processed and applied to FEA. As the nominal strain and nominal stress data must be processed during the back analysis, various theories can be applied depending on the material. Accordingly, the study proposed a basic inverse method that did not consider the ambient temperature or test speed.

The theories for the inverse method could be presented with the Hollomon (Equation. (5)), Ludwik (Equation. (6)), and Swift (Equation. (7)) models. As the back analysis theory generally dealt with only the plastic region after the yield stress, the strain value at the yield point was assumed to be zero (0). Therefore, a value that was lower than the yield stress could be generated in the low strain region using the Hollomon equation.

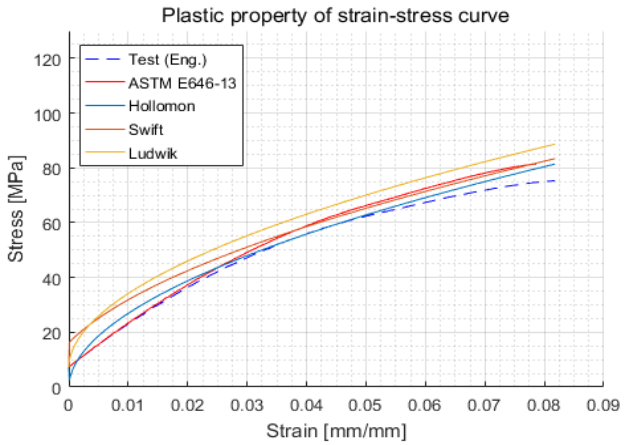

Figure-3. Calibration of eng. s-s curve and true s-s curve to apply MAT 24.

The Ludwik equation compensated for this error with the yield stress, while the Swift equation compensated for it with the yield strain. The parameters applied to each equation were the material parameter, and different values could be applied depending on the inverse method. K and nwere the strength coefficient and work hardening exponent, respectively according to ASTM E646-13.The following equation could be generated when the number of data points was N.

$$y = \log \sigma \quad (8)$$

$$x = \log \varepsilon \quad (9)$$

$$\mathrm{n} = [\{\mathrm{N} \sum xy\} - \{\sum x \sum y\}]/\{\mathrm{N} \sum x^2 - (\sum x)^2\} \quad (10)$$

$$\mathrm{b} = (\sum y /N) - (n \sum x /N) \quad (11)$$

$$\mathrm{K} = 10^{\mathrm{b}} \quad (12)$$

3. NON-LINEAR ANALYSIS

3.1. Finite element model

The finite element model used in the study consisted of a square element, and a size value of 2 to 14 divisions was considered based on the width () of the specimen center. The FEA solver considered both the implicit and explicit environments of LS-Dyna, and the eng. s-s curve of GFRP wt20% was applied to MAT24. For element formulation, the 2D shell type fully integrated method was applied.

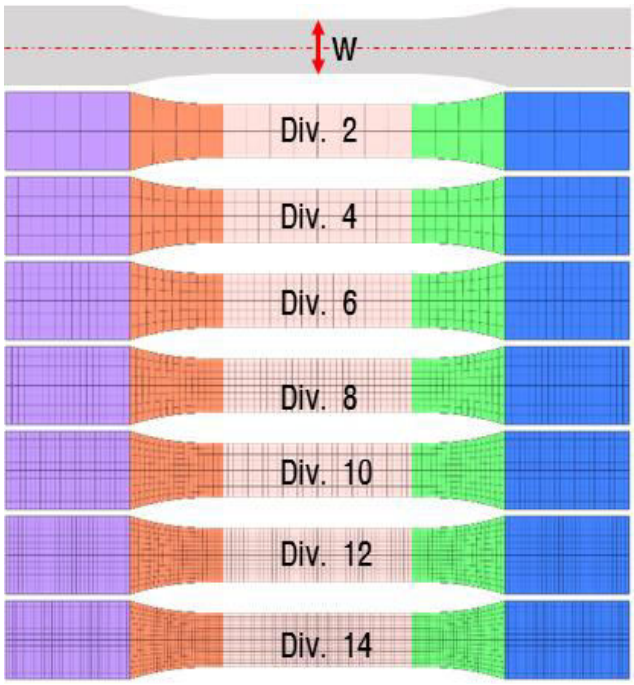

Figure-4. Finite element models based on the number of width divisions.

3.2. Finite element analysis

The non-linear FEA result of the tensile specimen is shown in Figure-5. The experimental data are indicated by dotted lines while the explicit and implicit FEA results are indicated by continuous lines. The analysis results showed that the precision around the yield point improved as the element size of the implicit FEA became smaller, and the graphs overlapped because the data were very similar except around the yield point. It was found that the explicit FEA result did not meet expectations as the element size became smaller. It was believed that this was a chronic issue with the explicit analysis method that did not consider convergence despite the error, and the error accumulated because of many elements. The error occurrence could be addressed with an error correction algorithm that exists in all FEA software. When this type of secondary issue is not considered, however, only implicit analysis can be considered to perform material property analysis.

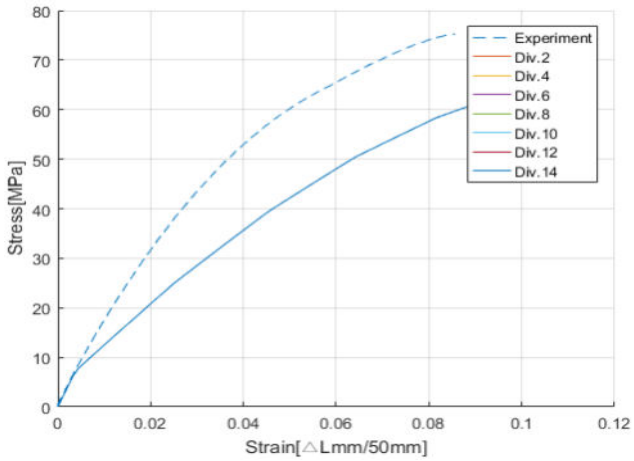

(a) The implicit FEA results

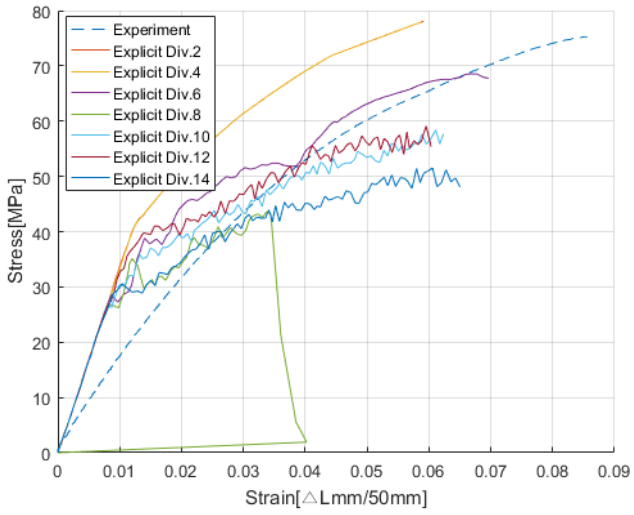

(b) The explicit FEA results

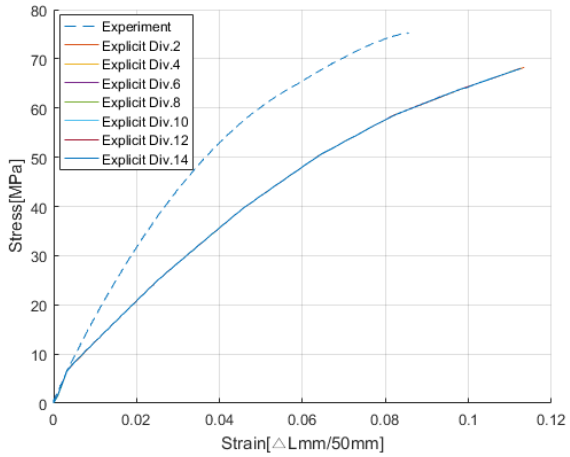

(c) The advanced explicit FEA results

Figure-5. FEA results after application of the eng. s-s curve.

Figure-6 shows the result of the FEA where the inverse method was applied. The accuracy of the analysis results by the inverse method could be achieved through comparison with the experimental data. OOO was the number used to discriminate the inverse method.

$$(\bar{e})_{\mathrm{q}} = \{\sum_{i=1}^{N}(|\sigma_s - \sigma_o|)_i\}/\mathrm{N}; \qquad \mathrm{q} = 1, \ldots, 3 \qquad (13)$$

$$(\bar{e})_{\mathrm{q}\%} = \{\sum_{i=1}^{N}(|\sigma_s - \sigma_o|/\sigma_o)_i\}/\mathrm{N}; \quad \mathrm{q} = 1, \ldots, 3 \qquad (14)$$

The analysis showed that the result of the inverse method that applied the Ludwik equation was the closest approximation to the actual specimen displacement value. However, it could be explained that the accuracy of the existing inverse method for GFRP was very low as the cumulative mean error was approximately 26%. In this case, parameter optimization could be considered. If the trend of the curve generated by the inverse method is optimized, a more accurate analysis result can be obtained.

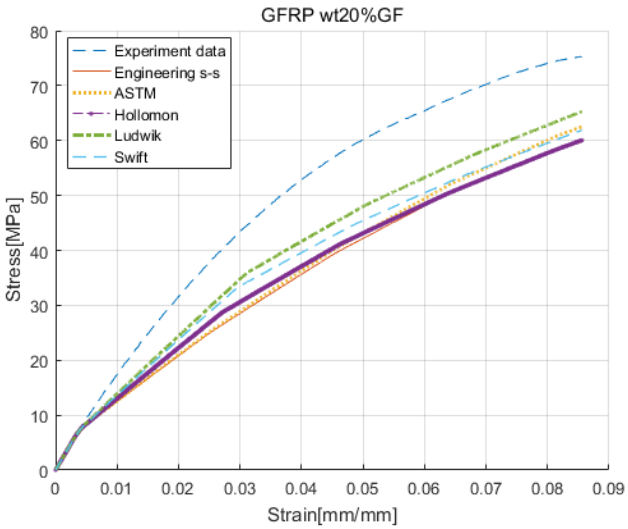

Figure-6. The eng. s-s curves of the experiment result and FEA result where back analysis was applied.

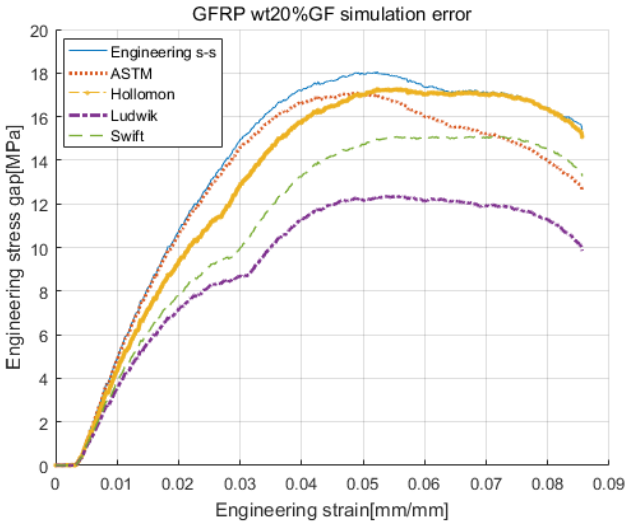

Figure-7. Difference between the FEA result and the experimental value.

Table-2. Error between the analysis results and experimental data.

q	Applied methods	$(\bar{e})_{\mathrm{q}}$[MPa]	$(\bar{e})_{\mathrm{q}\%}$[%]
-	Exp. eng. s-s curve	13.6987	27.1430
	D638-02a	12.7612	25.6553
1	Hollomon	12.8857	25.1020
2	Ludwik	9.1918	18.1953
3	Swift	11.0896	21.4932

4. PARAMETER OPTIMIZATION OF INVERSE METHOD

4.1. Optimization

The study involved error minimization for analytic simulations of the nominal strain-nominal stress generated by experiments. If the number of experimental data points was not the same as the analysis data points, a large error could occur in the process of obtaining the error value. Thus, only the X axis-plastic region of the experimental data was divided into eight values to establish the baseline. The eight values produced (with the plastic region divided into 12.5% portions each) were the number of general data points required by the material card of the FEA program. Therefore, the plastic region could be divided into a smaller region depending on the analysis environment. As the FEA results were more specific than the experimental data, the study explored and compared the most approximate data to the baseline of the experimental data and subsequently obtained the error. Formulation can be carried out when the design goal, restraints, and the design parameter range are determined to perform optimization.

Find
$x \in R^3$
$x = \{K\ n\ c\}$ (15)

Minimize
$f(x) = (\bar{e})_q$ (16)

Subject to
$g_{stress}(x_i) \leq (\sigma_o)_j\ ; j = 1, \ldots, 8$ (17)

$\{x_1 - (0.3x_1)\} \leq x_1 \leq \{x_1 + (0.3x_1)\}$ (18)

$\{x_2 - (0.3x_2)\} \leq x_2 \leq \{x_2 + (0.3x_2)\}$ (19)

$0.0005 \leq x_3 \leq 0.002$ (20)

4.2. Parameter optimization

DOE (design of experiment) was applied to the optimization process to minimize the number of analysis points. Numerically, the optimization process generated the error range from the baseline and calibrated the parameters repeatedly to improve convergence. Therefore, the optimization process was repeated for a maximum of 10 times without any limit for the error. Table-5 provides the optimized parameters of the inverse method resulting from the optimization process.

Table-3. Optimized analysis results.

Name	$(\bar{e})_q$ [MPa]	$(\bar{e})_{q\%}$ [%]	K [MPa]	n	C
Hollomon	1.5445	3.9680	309.843	0.4119	-
Ludwik	0.7909	2.0230	268.845	0.45536	19.3
Swift	0.8289	2.3928	258.761	0.36595	0.002

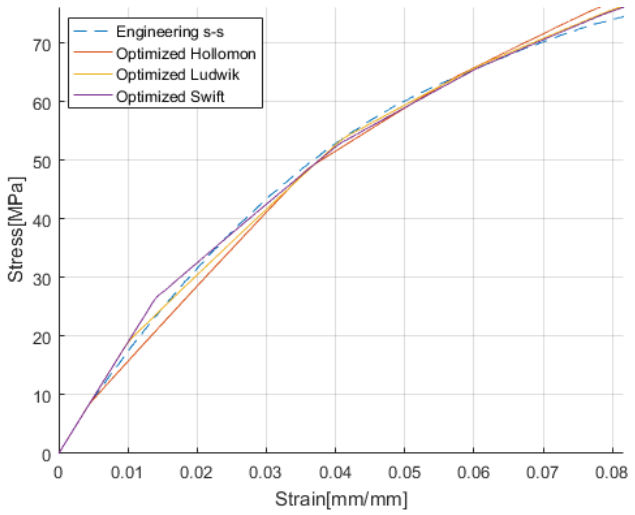

Figure-8. Nominal strain-nominal stress of the optimized models.

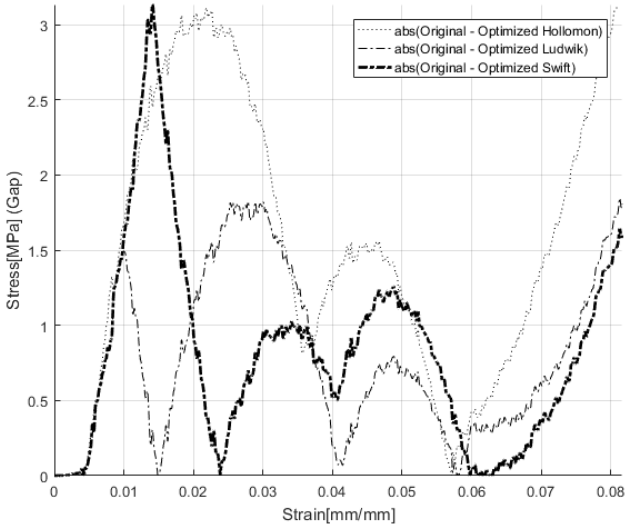

Figure-9. Error of the optimized model.

5. RESULTS AND DISCUSSIONS

Figure-8 presents the FEA result where optimized parameters were applied. It suggests that the optimized inverse method could explain the actual displacement more accurately than the FEA with the inverse method, shown in Figure-6. The parameters could be calibrated within 30% from the existing baseline. Figure-9 demonstrates the error between the optimized analysis result and experimental value. The difference between the optimized inverse method result and experimental data was a maximum of 12% and 2–3% on average. The accuracy improved by 24% compared to the non-optimized inverse methods.

6. CONCLUSIONS

This study proposed a method to reduce the error between the eng. s-s curve obtained by testing and the eng. s-s curve generated by FEA, by applying the inverse methods and a DOE optimization method to the GFRP tensile specimen model. The FEA result showed that the existing inverse methods were inappropriate for nonlinear FEA, and parameter optimization was applied to the inverse methods to reduce the error. A new inverse method needs to be developed that can replace the existing inverse methods and reduce the error. Consequently, a study on the inverse method that reflected environmental factors such as the tensile test speed and process condition can consider [16]. It is believed that the study result can be considered to predict the axial displacement of GFRP in the macroscopic stage to obtain material properties.

ACKNOWLEDGEMENTS

This work was supported by the Human Resource Training Program for Regional Innovation and Creativity through the Ministry of Education and National Research Foundation of Korea (NRF-2015H1C1A1035950) and the Ministry of Trade, Industry & Energy (MOTIE), Korea Institute for Advancement of Technology (KIAT) through the Encouragement Program for The Industries of Economic Cooperation Region

REFERENCES

[1] M.S. Joun, J.G. Eom, M.C. Lee. 2008. A new method for acquiring true stress-strain curves over a large range of strains using a tensile test and finite element method. Mechanics of Materials. 40: 586-593.

[2] ASTM D638-02a. Standard Test Method for Tensile Properties of Plastics.

[3] Mark A. Iadicola. 2011. Validation of Uniaxial Data beyond Uniform Elongation. KSTP. pp. 742-749.

[4] M. Geiger, W. Hubnatter, M. Merklein. 2005. Specimen for a novel concept of the biaxial tension test. Journal of Materials Processing Technology. 167: 177-183.

[5] Feipeng Zhu, Pengxiang Bai, Jingbin Zhang, Dong Lei, Xiaoyuan He. 2015. Measurement of true stress strain curves and evolution of plastic zone of low carbon steel under uniaxial tension using digital image correlation. Optics and Lasers in Engineering. 65: 81-88.

[6] J. H. Kim, A. Serpantie, F. Barlat, F. Pierron, M.G. Lee. 2013. Characterization of the post-necking strain hardening behavior using the virtual fields method. International Journal of Solids and Structures. 50: 3829-3842.

[7] M.S. Joun, J.G. Eom, M.C. Lee. 2008. A new method for acquiring true stress–strain curves over a large range of strains using a tensile test and finite element method. Mechanics of Materials. 40: 586-593.

[8] Masayuki Kamaya, Masahiro Kawakubo. 2011. A procedure for determining the true stress–strain curve over a large range of strains using digital image correlation and finite element analysis. Mechanics of Materials. 43: 243-253.

[9] Kunmin Zhao, Limin Wang, Ying Chang, Jianwen Yan. 2016. Identification of post-necking stress–strain curve for sheet metals by inverse method. Mechanics of Materials. 92: 107-118.

[10] J.M. Park, H.S. Seo, M.H. Kwon, J.H. Lim. 2014. Experimental Study on the Material Characteristics of Glass Fiber Composties. Journal of Korean Society Advanced Composite Structure. 5(1): 16-21.

[11] JorgHohe, Carla Beckmann, Hanna Paul. 2015. Modeling of uncertainties in long fiber reinforced thermoplastics. Materials and Design. 66: 390-399.

[12] Osman Unal, Fuat Demir, Tayfun Uygunoglua. 2007. Fuzzy logic approach to predict stress-strain curves of steel fiber-reinforced concretes in compression. Building and Environment. 42: 3589-3595.

[13] ASTM E646-07. Tensile Strain-Hardening Exponents (n-values) of Metallic Sheet Materials.

[14] Banabic D. 2010. Sheet Metal Testing and Flow Curve Determination under Multiaxial Conditions. Advanced Engineering Materials.

[15] Kleemoloa, Nieminen. 1974. On the strain-hardening parameters of metals. Metallurgical and Materials Transactions B. 5(8): 1863-1866.

[16] S.B. Kim, H. Huh, D.O. Kim, M.B. M. 2005. Evaluation of Dynamic Tensile Characteristics of the High Strength Steel Sheet for an Auto-body. The Korean Society of Mechanical Engineering. pp. 1654-1659.